Int. J. Heat Mass Transfer. Vol. 26, No. 7, pp. 1069–1074, 1983
Printed in Great Britain

0017-9310/83 $3.00 + 0.00
Pergamon Press Ltd.

LOW PRANDTL NUMBER CONVECTION BETWEEN DIFFERENTIALLY HEATED END WALLS

J. E. HART
Department of Astrogeophysics, University of Colorado, Boulder, CO 80309, U.S.A.

(*Received* 1 *February* 1982 *and in final form* 1 *December* 1982)

Abstract—Two-dimensional convection in a horizontal cavity of height D and length L, driven by differential heating of the two vertical end walls, is described. Of particular interest is the range of external parameters, at low Prandtl numbers, for which the circulation contains a parallel flow core. The simple core solution, asymptotically valid at small aspect ratio D/L, breaks down either as end effects extend into the center of the cavity, or as a secondary shear flow instability develops in the core itself.

NOMENCLATURE

- D, fluid depth;
- Gr, Grashof number;
- g, gravitational acceleration;
- i, $(-1)^{1/2}$;
- L, length between end walls;
- Nu, Nusselt number;
- Pr, Prandtl number;
- Ra, Rayleigh number;
- T, temperature;
- ΔT, imposed external temperature difference;
- u, horizontal velocity;
- $\mathbf{v}$, velocity vector;
- w, vertical velocity;
- x, horizontal coordinate;
- z, vertical coordinate.

Greek symbols

- α, coefficient of thermal expansion;
- ε, container aspect ratio;
- κ, thermal diffusivity;
- ψ, two-dimensional stream function;
- π, pi (3.141592);
- ν, kinematic viscosity.

Subscripts

- j, homogeneous solution index.

1. INTRODUCTION

THERE has been considerable recent interest in thermally driven flows in rectangular cavities in which the heating is imposed differentially on the two end walls. For any small non-zero temperature contrast there will be a general unicellular motion up the hot wall, across the top of the container, down the cold wall, and returning across the bottom. The single cell circulation that forms in response to the lateral temperature gradient generated by diffusion of heat in from the sides has come to be known as a Hadley circulation, after Hadley [1] who proposed such a thermally direct unicellular model for the circulation of the earth's atmosphere, although such flows clearly arise in many important non-geophysical applications. This paper describes the development of the unicellular flow and secondary instability of the unicell for shallow cavities filled with a low Prandtl number liquid. Such flows occur in typical crystal growth experiments [2], and it is of interest to extend earlier work on flows in shallow cavities of moderate Prandtl number liquids to the low Prandtl number limit.

For a cavity of depth D and length L, the structure of the unicell and the evolution of the flow in general depend on the aspect ratio $\varepsilon \equiv D/L$, and the Grashof number $Gr = g\alpha\Delta T D^3/\nu^2$, using the standard nomenclature given below. Hart [3] showed that shallow ($\varepsilon \ll 1$) Hadley circulations would have a core flow away from the end walls that was of a particularly simple form; basically a cubic velocity profile $U(z)$ associated with a thermal field of form $T \sim x + f(z)$, where z is the height and x the distance horizontally from one of the end walls. This circulation was thought to be valid outside a distance of order D from either end provided Gr and ε were small enough. Cormack, Leal, and Imberger [4], henceforth denoted CLI, argued that the strength of the core circulation should depend on the flow in the end regions, and used a matching procedure that connects these two flows to determine the amplitude of the parallel flow, and hence the Nusselt number. Their solution is based on a small ε expansion. Formally, Gr and the Prandtl number Pr (and hence the Rayleigh number $GrPr$) are held fixed and are of order one, although their series may converge for larger values. This ordering leads to the major consequence that the end regions of the cavity are basically diffusive. This means that the penetration of the end effects into the core is dominated solely by geometry. That is, the end regions penetrate a distance of order D into the core independent of Gr and Pr. We are interested in relatively large Gr flows in which inertia will be of fundamental importance near the ends. How the momentum advection terms affect the end-core matching, and how they modify the end influence length are two major topics of this paper.

The CLI model, and the more recent approximate model of Bejan and Tien [5] that uses a roughly diffusive test function solution in the turning regions, do not allow for secondary motions in either the ends or

the core. These are especially important at low Prandtl number and can only be investigated using a model that retains the full effect of the inertial terms in the basic equations. Only then can the importance of the corners at finite ε and large Gr be understood. In the following we shall try to delineate the range of ε and Gr for which a parallel flow core may exist, and whether or not it is end effects or secondary instability that causes its breakdown.

2. THE MODEL

We consider the steady 2-dim. flow of a Boussinesq liquid in the geometry shown in Fig. 1. The governing Navier–Stokes equations are non-dimensionalized using scales ΔT, $g\alpha\Delta TD^2/\nu L$ and D, for temperature, velocity, and length, respectively. The normalized equations then become

$$\varepsilon\nabla^2\omega + T_x = Gr\,\varepsilon^2 J(\psi,\omega), \tag{1}$$

$$\nabla^2\psi = \omega, \tag{2}$$

$$\nabla^2 T = Ra\,\varepsilon J(\psi,T), \tag{3}$$

$$u = -\psi_z, \quad w = \psi_x, \tag{4}$$

$$J(f,g) = f_x g_z - f_z g_x, \tag{5}$$

$$\nabla^2 \equiv \partial^2/\partial x^2 + \partial^2/\partial z^2 \tag{6}$$

with $Gr = g\alpha\Delta TD^3/\nu^2$, the Grashof number, $Pr = \nu/\kappa$, the Prandtl number, and $Ra = GrPr$, the Rayleigh number. We have previously defined $\varepsilon = D/L$ as the aspect ratio. In the above ν is the kinematic viscosity, κ the thermal diffusivity, g the gravitational acceleration, and α the coefficient of thermal expansion. ΔT is the applied thermal contrast. Referring to Fig. 1, the boundary conditions become

$$T(0,z) = T_z(x,1/2) = T_z(x,-1/2) = 0, \tag{7}$$

$$T(\varepsilon^{-1},z) = 1 \tag{8}$$

with velocity v and streamfunction ψ both equal to zero on all the boundaries. Thus we are considering rigid impermeable walls, conducting on the ends and insulating on the top and bottom.

Hart [3] first noted a simple exact parallel flow core solution to equations (1) and (2). This solution is

$$\psi_c = a(z^2/48 - z^4/24 - 1/384) \tag{9}$$

and

$$T_c = a\varepsilon x + b + Ra\,\varepsilon^2 a^2 F(z) \tag{10}$$

with

$$F(z) = z^5/120 - z^3/144 + z/384.$$

Here a and b are constants that in principle must be obtained by matching this core flow to the flow in the end regions near $x = 0$ and $x = \varepsilon^{-1}$. The core solution describes a simple cubic velocity counterflow driven by a constant lateral temperature gradient that for low Gr has diffused into the core from the ends. At higher Gr transients will be advective, but the constant x-gradient represents a constant diffusive flux through the core. There is also an advective heat flux, independent of x in the core, that is partially balanced by vertical heat diffusion. This latter effect leads to the z dependence of T_c.

The end regions influence the core in two ways. Firstly through the constants a and b, and secondly through the core influence length. The latter is simply the distance over which significant non-parallel flow occurs for $x \sim 0$ in a very shallow cavity. It is simplest to assume that the flow in the end region near $x = 0$ will match the parallel flow core for sufficiently large x in an infinitely long cavity. Formally, we wish to solve equations (1)–(3) in the left hand end region under the condition that as x becomes very large the end flow variables ψ and T become independent of x and asymptotically match equations (9) and (10). Then the region over which x variations are significant determines the influence-length of the ends, or equivalently how shallow a cavity must be to observe a parallel flow core near the center. Note that this conversion from a closed to an open boundary value problem eliminates explicit dependence on the aspect ratio ε, and so decreases the dimension of the external parameter space by one, a distinct advantage since numerical techniques are employed.

Thus we must solve equations (1)–(3) subject to

$$T(x\to\infty,z) = T_c(x,z), \tag{11}$$

$$\psi(x\to\infty,z) = \psi_c(z) = aH(z) \tag{12}$$

and

$$\psi(0,z) = \psi_x(0,z) = \psi(x,\pm\tfrac{1}{2}) = \psi_z(x,\pm\tfrac{1}{2}) = T(0,z) = T_z(x,\pm\tfrac{1}{2}) = 0. \tag{13}$$

The problem can be simplified somewhat by writing

$$T = a\varepsilon x + a\varepsilon\hat{R}T'(x,z) \tag{14}$$

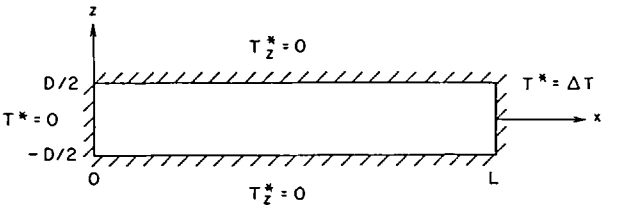

FIG. 1. Geometry for the problem, showing thermal boundary conditions. The cavity is assumed infinite in y, with rigid boundaries as indicated.

and

$$\psi = a\psi'(x,z) \tag{15}$$

while at the same time defining new Rayleigh and Grashof numbers

$$\hat{R} \equiv Ra\,\varepsilon a, \tag{16}$$

$$\hat{G} \equiv Gr\,\varepsilon a. \tag{17}$$

The transformed problem and boundary conditions are now

$$\nabla^2\omega' + \hat{R}T_x' + 1 = \hat{G}J(\psi',\omega'), \tag{18}$$

$$\nabla^2 T' = -\psi_z' + \hat{R}J(\psi',T'), \tag{19}$$

$$\nabla^2\psi' = \omega', \tag{20}$$

with

$$\psi'(x\to\infty,z) = H(z), \tag{21}$$

$$T'(x\to\infty,z) = c^*/\hat{R} + F(z) \tag{22}$$

along with the homogeneous boundary conditions. The centro-symmetry constraint that $T_c(\frac{1}{2},0) = \frac{1}{2}$ gives $a = 1-2b$. Integrating equation (19) from $z = -\frac{1}{2}$ to $z = +\frac{1}{2}$ and then from $x = 0$ to $x = \infty$, using the boundary conditions in several integrations by parts, we find

$$c^* = \hat{R}^2 Q(\hat{R},\hat{G}) \tag{23}$$

where

$$Q = \int_{-\frac{1}{2}}^{+\frac{1}{2}} dz \int_0 \hat{u}\hat{T}\,dx \tag{24}$$

with $\hat{u}$ and $\hat{T}$ being those parts of u' and T' that are functions of x and z, for example $\hat{\psi} = \psi' - H(z)$ with $u' = -\psi_z'$. The core solution amplitude a is now given by the implicit relationship

$$a = 1 - \frac{2\varepsilon^3 Ra^2 a^2 Q}{1+2\varepsilon^3 Ra^2 a^2 Q}. \tag{25}$$

Combining equations (25), (24) and (16) yields $c^*(a,\varepsilon)$. Equation (25) is exact, though $Q(\hat{R},\hat{G})$ needs to be determined from the numerical solution of the above problem. Note that the CLI expansion gave only the first approximation to this equation,

$$a = 1 - 2\varepsilon^3\, Ra^2\, Q \tag{26}$$

with their value of Q being obtained by numerical integration of a different reduced problem. Further comparisons are given in the discussion section.

The numerical solution of equations (18)–(20) is accomplished by solving a sequence of Poisson equations in which the RHSs of the equations are relaxed upwards from zero to their final values. Separate calculations using a time dependent code verified the time independence for the extreme G values cited here. An inner iteration of equation (20) along with an application of the induced boundary vorticity, for example

$$\omega'(0,z) = 2\psi'(\Delta x,z)/\Delta x^2,$$

assures that the no-slip condition is satisfied. The grid size is chosen to adequately resolve any viscous region. Typically this involves 25 points in z. The mesh is uniform and enough points are taken in x so that the solutions become independent of x well before the right hand computational boundary. The actual grids involved between 97 and 250 points in x. The Jacobians were written using second-order differences in conservative form, while the Poisson equations were solved by a combined Fast Fourier Transform and tri-diagonal matrix inversion method. Since the numerical solution yields the predicted flow field as a function of $\hat{R}$ and $\hat{G}$, it is most convenient to think of equation (25) as an explicit equation for $a(\hat{R},\hat{G},\varepsilon)$. As stated above, this relationship is exact, involving no approximation other than numerical discretization. Thus by solving the numerical problem for a range of Pr and $\hat{G}$, a relationship can be easily built up that gives $a(Gr, Ra, \varepsilon)$.

3. DISCUSSION OF RESULTS

A fairly extensive set of integrations of the end region equations were carried out for values of $\hat{G}$ between 100 and 100 000, the latter value being well into the régime with secondary vortices superimposed on the flow for all x. That is, for these cases, the solution cannot be made x-independent at large x since any attempt to lengthen the domain just adds more vortices. Prandtl numbers between 0.1 and 0.001 were chosen.

We first compare our solutions with those of CLI. For small $\hat{R}$ and $Pr \leqslant 0.1$ we find that $2Q = 3.44 \times 10^6$, roughly independent of $\hat{R}$ and Pr. Using the expanded equation (26), and CLI's value $2Q = 3.48 \times 10^{-6}$, we see that the results agree to within about 1%. This is certainly within the range of numerical error. A further check on the model can be obtained by performing some solutions in a closed domain of aspect ratio 0.1. That is, we effectively solve the completely non-linear problem as originally posed with zero velocity and streamfunction conditions at $x = 1/\varepsilon$ instead of the asymptotic condition of the reduced problem. We then can compare the prediction of the Nusselt number

$$Nu \equiv \int_{-\frac{1}{2}}^{+\frac{1}{2}} \partial T/\partial x|_0\, dz/\varepsilon \tag{27}$$

with the numerical study of Shiralkar and Tien [6]. This comparison is shown in Table 1. There is good

Table 1. Nusselt number in a cavity with $\varepsilon = 0.1$ (results of Shiralkar and Tien [6] in parentheses)

	Ra		
Pr	10^3	10^4	10^5
0.1	1.026 (1.03)	2.81 (3.01)	19.06 (18.65)
0.03	1.026 (1.03)	2.39 (2.62)	11.69 (13.20)
0.01	1.029 (1.02)	1.21 (1.96)	

agreement between the two models for $Pr = 0.1$. At the lower values of Pr the models agree at low Ra, but at moderate to high values the present study predicts a significantly lower Nusselt number. At these parameter settings there are very strong secondary vortices in the solutions. Heat is passed from cell to cell. This is a less efficient process than for one unicell. Shiralkar and Tien noticed the presence of very weak secondary motions in the core of their low Prandtl number high Rayleigh number computations [9]. The absence of the strong vortices found here was apparently due to the nature and resolution of their difference approximations in the core of the cavity. The suppression of the shear instability modes lead to higher heat fluxes at these parameter settings.

Figure 2 shows streamlines and T' contours for $\hat{G}$ small enough for the velocity field to be essentially viscous. The solutions shown in Figs. 2(a) and 2(b) are close to the asymptotic limit of CLI. However, note that if Pr is only moderately small [Fig. 2(c)], there is a substantial asymmetry in the thermal field. As $\hat{G}$ is increased to around 7000 (Fig. 3), the velocity field begins to show some effects of inertial accelerations into the upper left-hand corner along with the formation of a single cat's eye at mid-depth. The cat's eye weakens as the Prandtl number is increased. This is related to the rise in thermal vertical stability [see equation (10)] with Pr, and the associated suppression of vertical velocities away from the end walls where they are forced on the flow by the geometry.

Hart [3] shows that for $Pr < 0.02$ or so, the critical $\hat{G}$ value for the onset of stationary secondary vortices by shear flow instability on the parallel core profile is $\hat{G} = 7980$. This critical value comes from a linear stability theory assuming a parallel basic flow infinite in the x direction. Thus it does not reflect any end influence. Figures 4(a)–(c) shows how the streamline

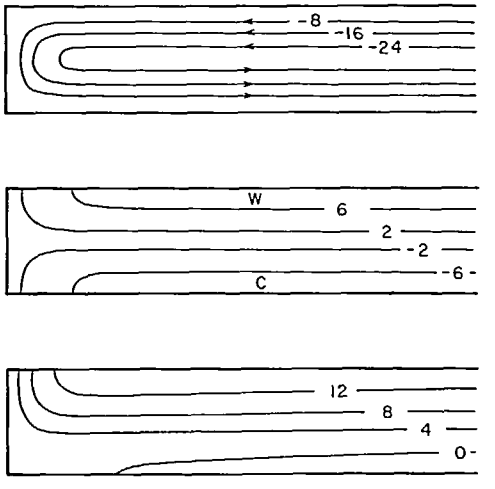

FIG. 2(a). ψ' for $\hat{G} = 500$. Contour labels scaled up by 10^4. (b) T' for $\hat{G} = 500$, $Pr = 0.01$. Label scale factor 10^4. (c) T' for $\hat{G} = 500$, $Pr = 0.1$. Label scale factor 10^4. Aspect ratio 1/7, numerical grid 25 × 169.

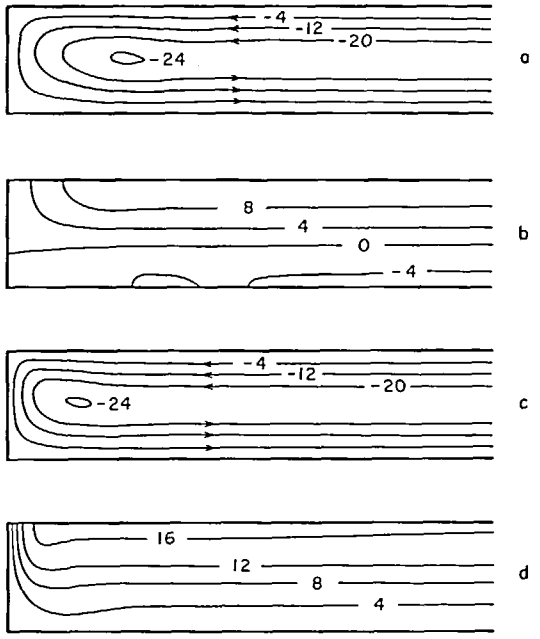

FIG. 3 (a) and (b). ψ' and T' for $\hat{G} = 6900$, $Pr = 0.25$. Label scale factor for (a) = 10^4 and for (b) = 10^3. (c) and (d) ψ' and T' for $\hat{G} = 6900$, $Pr = 0.2$. Same contour labels as in (a) and (b). Numerical grid 25 × 169.

patterns evolve as $\hat{G}$ is increased upwards past this critical value.

The sequence of streamline pictures indicates that if one were to measure instability by looking for patterns of upward velocity to the left of $x = \frac{1}{2}\varepsilon$ then obviously one would conclude that the cavity flow was 'unstable' for $\hat{G}$ below $\hat{G}_c$. More correctly, the secondary cats-eye vortices grow smoothly and monotonically with increasing $\hat{G}$, although there is a steep increase in their amplitude at the critical value for plane parallel flow. If there were no end walls, the upward velocity would be zero until $\hat{G} = \hat{G}_c$, whence it would increase as $(\hat{G} - \hat{G}_c)^{1/2}$. The smooth transition in the cavity is an example of an imperfect bifurcation. Similar processes have been described in other contexts [7]. In Fig. 4 the fact that we force a matching to the core solution at the right-hand boundary probably modulates the solution somewhat, although for the supercritical $\hat{G}$, and the extreme aspect ratio used, this effect is reasonably small.

The origins of the imperfect bifurcation, i.e. the cat's eye in the corner, lie, at very small $\hat{G}$, in the fact that solutions of the forced Stokes problem have eigenfunctions in x that oscillate down the cavity. This effect was first noted by Moffat [8]. For example, solving

$$\nabla^4 \psi = -1$$

with free boundaries at $z = \pm\frac{1}{2}$ leads to homogeneous components with form

$$\psi_j = a_j \, e^{r_j x} \cos(j\pi z/2)$$

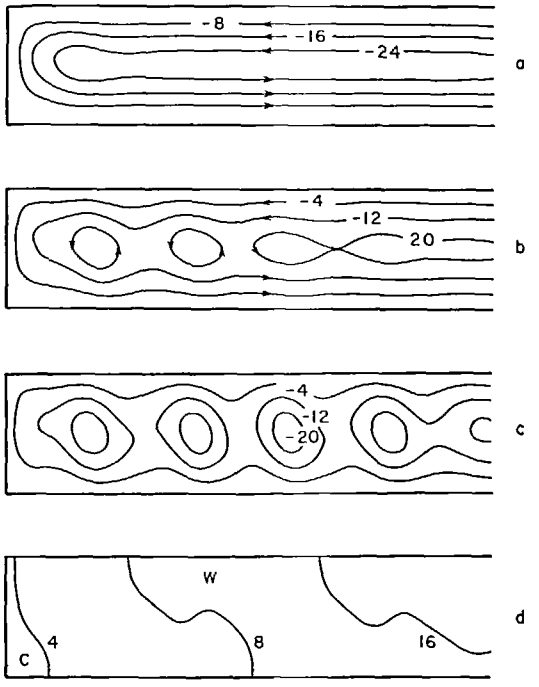

FIG. 4. ψ' fields for $\hat{G} = 6900$ (a), 8400 (b), and 11 900 (c). Labels scaled by 10^4. T' for $\hat{G} = 11\,900$, $Pr = 0.1$ (d). Labels scaled by 10^3.

with

$$r_j^2 = j^2\pi^2(1 \pm i\sqrt{3})/2.$$

The viscous eddies or recirculations are extremely weak, but are enhanced by negative vorticity advection into the turning region from the core flow near $z = 0$. The secondary end eddies are independent of the thermal field for the lowest Prandtl numbers considered in this paper, but weaken with increasing Pr as noted above.

For low Pr though, we have seen that the core solution does not exist for $\hat{G}$ above about 7900. Any attempt to estimate Nu from a core-corner matched approximation will probably be in error at values of $\hat{G}$ in excess of this number. However, since $\hat{G} = Gr\,a\varepsilon$ one needs to discuss how a varies with $\hat{G}$ and Pr before the critical value can easily be related to the physical external parameters.

Table 2 shows some calculated values of the Q function of (2.24) for values of $\hat{G}$ at or below the critical number. Obviously for values of $\hat{G}$ above 8000 or so, a matching to the core solution cannot be obtained anyway. As the problem has been normalized, Q depends only weakly on $\hat{G}$ and Pr. One can thus calculate a to within about 5% for any $\hat{G}$ less than 6000 by setting $Q = 1.78 \times 10^{-6}$ in equation (25). This then leads to Fig. 5 that gives a as a function of $Ra^2\varepsilon^3$. There are two constraints on the general use of this figure. First, if the value of $\hat{G} = Ra\,a\varepsilon/Pr$ is greater than 8000 ($0.001 \lesssim Pr \lesssim 0.1$) the core solution will not exist because of secondary vortices and the value of a is irrelevant. Secondly, the value of ε must be low enough that the center of the cavity falls outside the end region influence length. Table 3 gives the required values of $\varepsilon \equiv \varepsilon_c$ for several Pr. For $Pr < 0.02$ the required aspect ratios are essentially those given for $Pr = 0.025$.

Table 2. Values of $Q(\hat{G}, Pr)$

	$Q(\hat{G}, Pr) \times 10^6$		
$\hat{G}$	$Pr = 0.001$	$Pr = 0.01$	$Pr = 0.1$
500	1.72	1.71	1.70
1000	1.72	1.71	1.70
2000	1.74	1.73	1.71
4000	1.81	1.80	1.74
8000	2.23	2.21	2.06

Figure 5 is most useful in evaluating the effective internal Grashof number $\hat{G}$ in terms of external parameters. Unless $Ra^2\varepsilon^3$ is greater than 10^5, $\hat{G} \doteq Gr\,\varepsilon$. It is clear that for low Pr, secondary vortices will upset the unicellular core before a becomes less than one, unless ε approaches one itself. In this instance the core will not exist either because of the influence length and proximity of the two ends.

One can also use Fig. 5 to estimate the Nusselt number. In terms of the constant a,

$$Nu = a + 2.75 \times 10^{-6}\,Ra^2\varepsilon^2a^3. \qquad (28)$$

However, note that this figure is a prediction of a assuming constant Q. Thus a is good to about 10%, and Nu is more approximate, because of the cubic term in a, when Nu is significantly larger than one. For example, at $Ra = 10^4$, $\varepsilon = 0.1$, and $Pr = 0.1$ (a case with very weak secondary vortices) Nu is predicted to be 2.24. This can be compared with the full box calculation value of 2.81 (Table 2). Even though these parameter settings do not satisfy the aspect ratio requirements very well, the agreement is reasonable.

In conclusion we have shown that for Prandtl numbers less than about 0.1, and aspect ratios less than the same value, a parallel flow core will exist with approximately unit non-dimensional amplitude ($a = 1$) up to the point ($Gr \sim 8000$) where secondary vortices appear. The secondary circulations propagate out from the ends, as $\hat{G} = Gr\,\varepsilon a$ is increased, as an imperfect bifurcation.

Table 3. Critical aspect ratios

	$\varepsilon_c(\hat{G}, Pr)$		
$\hat{G}$	$Pr = 0.025$	$Pr = 0.05$	$Pr = 0.125$
500	0.59	0.52	0.41
2000	0.60	0.50	0.39
4800	0.15	0.12	0.095
6900	0.13	0.099	0.082

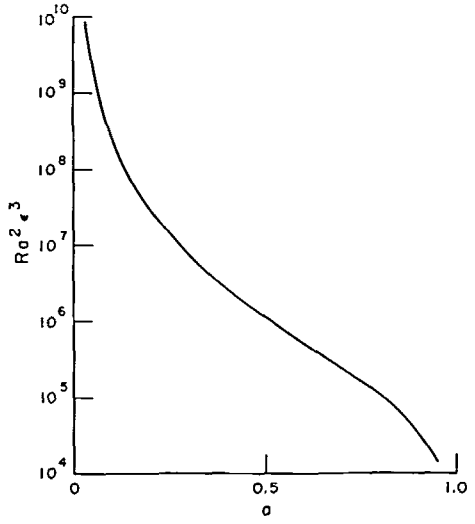

FIG. 5. Equation (25) using a constant value of $Q = 3.5 \times 10^{-6}$.

Acknowledgements—This research was sponsored by NSF grant ATM8111718, and NASA contract NAS-8-31958. The author would like to thank Dr D. R. Moore for donating three extremely efficient Poisson solving routines, and for some stimulating discussions on imperfect bifurcations.

REFERENCES

1. G. S. Hadley, Concerning the cause of the general trade winds, *Phil. Trans.* **29**, 58-62 (1735).
2. D. T. J. Hurle, Temperature oscillations in molten metals and their relationship to the growth state in melt grown crystals, *Phil. Mag.* **13**, 305–310 (1966).
3. J. E. Hart, Stability of thin non-rotating Hadley circulations, *J. Atmos. Sci.* **29**, 687–697 (1972).
4. D. E. Cormack, L. G. Leal and J. Imberger, Natural convection in a shallow cavity with differentially heated end walls. Part 1: Asymptotic theory, *J. Fluid Mech.* **65**, 209–229 (1974).
5. A. Bejan and C. L. Tien, Laminar natural convection heat transfer in a horizontal cavity with different end temperatures, *J. Heat Transfer* **100**, 641–647 (1978).
6. G. S. Shiralkar and C. L. Tien, A numerical study of laminar natural convection in shallow cavities, *J. Heat Transfer* **103**, 226–231 (1981).
7. P. Hall and I. C. Walton, Benard convection in a finite box: secondary and imperfect bifurcations, *J. Fluid Mech.* **90**, 377–395 (1979).
8. H. K. Moffat, Viscous and resistive eddies near a sharp corner, *J. Fluid Mech.* **18**, 1–18 (1964).
9. C. L. Tien, personal communication (1982).

CONVECTION A FAIBLE NOMBRE DE PRANDTL ENTRE DES PAROIS CHAUFFEES DIFFEREMMENT

Résumé—On décrit la convection bidimensionnelle dans une cavité horizontale de hauteur D et de longueur L, créée par un chauffage différent sur des parois en bout verticales. On porte intérêt au domaine de paramètres externes, à faible nombre de Prandtl, pour lequel la circulation contient un coeur à écoulement parallèle. La solution simple de coeur, anymptotiquement valable pour un rapport de forme D/L faible, disparait lorsque l'un ou l'autre des effets d'extrémité s'étend vers le centre de la cavité, ou lorsqu'une instabilité d'écoulement de cisaillement secondaire se développe dans le coeur même.

KONVEKTION ZWISCHEN UNTERSCHIEDLICH BEHEIZTEN SEITENWÄNDEN BEI KLEINER PRANDTL-ZAHL

Zusammenfassung—Es wird die zweidimensionale Konvektion in einem horizontalen Hohlraum mit der Höhe D und der Länge L infolge unterschiedlicher Beheizung der beiden vertikalen Seitenwände beschrieben. Von besonderem Interesse ist der Bereich von äußeren Parametern, bei kleinen Prandtl-Zahlen, für welchen sich im Kern eine parallele Strömung ausbildet. Die einfache Lösung für die Kernströmung, die für den Grenzfall eines kleinen Seitenverhältnisses D/L gültig ist, wird ungültig, entweder wenn sich die Randeinflüsse ins Zentrum des Hohlraums ausdehnen, oder wenn sich im Kern selbst durch eine sekundäre Scherströmung eine Instabilität entwickelt.

КОНВЕКЦИЯ МЕЖДУ РАЗЛИЧНО НАГРЕТЫМИ ТОРЦОВЫМИ СТЕНКАМИ ПРИ МАЛОМ ЧИСЛЕ ПРАНДТЛЯ

Аннотация—Описывается двумерная конвекция в горизонтальной полости высотой D и длиной L, возникающая из-за различного нагрева двух вертикальных торцовых стенок. Особый интерес представляет диапазон внешних параметров при малых числах Прандтля, для которых циркуляция содержит ядро потока. Простое решение для ядра, асимптотически справедливое при малом отношении D/L, перестает быть справедливым по мере того, как концевые эффекты начинают влиять на течение в центре полости, или по мере того, как возникает неустойчивость вторичного сдвигового потока в самом ядре потока.